

Dalton Transactions

Accepted Manuscript



This is an *Accepted Manuscript*, which has been through the Royal Society of Chemistry peer review process and has been accepted for publication.

Accepted Manuscripts are published online shortly after acceptance, before technical editing, formatting and proof reading. Using this free service, authors can make their results available to the community, in citable form, before we publish the edited article. We will replace this *Accepted Manuscript* with the edited and formatted *Advance Article* as soon as it is available.

You can find more information about *Accepted Manuscripts* in the [Information for Authors](#).

Please note that technical editing may introduce minor changes to the text and/or graphics, which may alter content. The journal's standard [Terms & Conditions](#) and the [Ethical guidelines](#) still apply. In no event shall the Royal Society of Chemistry be held responsible for any errors or omissions in this *Accepted Manuscript* or any consequences arising from the use of any information it contains.

1 **The catalytic performance of metal complexes immobilized on SBA-15 in the ring**
2 **opening polymerization of ϵ -caprolactone with different metals (Ti, Al, Zn and**
3 **Mg) and immobilization procedures**

4
5 Yolanda Pérez^{a*}, Isabel del Hierro^{a*}, Lydia Zazo^a, Rafael Fernández-Galán^b, Mariano
6 Fajardo^a

7
8 ^aDepartamento Biología y Geología, Física y Química Inorgánica (E.S.C.E.T.),
9 Universidad Rey Juan Carlos, 28933 Móstoles, Madrid, Spain. Tel.: (+34) 914887022
10 Fax: (+34) 914888143

11 E-mail: yolanda.cortes@urjc.es, isabel.hierro@urjc.es

12 ^bDepartamento Química Inorgánica, Orgánica y Bioquímica, Facultad de Ciencias y
13 Tecnologías Químicas, Universidad de Castilla-La Mancha, Campus Universitario de
14 Ciudad Real, 13071-Ciudad Real, Spain.

15
16 **Abstract**

17 A family of heterogeneous catalysts has been prepared employing different
18 strategies. Firstly by direct reaction or grafting of titanium, zinc, aluminium and
19 magnesium precursors with dehydrated SBA-15 and secondly by reaction of the
20 metallic derivatives with a hybrid SBA-15 mesoporous material, which possesses a new
21 covalently bonded linker based on an amino alcohol chelate ligand. These materials
22 have been characterized by X-ray diffraction (XRD), X-ray fluorescence (XRF), N₂
23 adsorption-desorption, FT-IR and multi nuclear NMR spectroscopy. The catalytic
24 performance of the prepared materials has been studied in the ring opening
25 polymerization of ϵ -caprolactone and compared with their homogenous counterparts.
26 Conversion values obtained by using homogeneous and heterogeneous catalysts depend
27 on the metal precursor and the synthetic procedure. The most active heterogeneous Ti-
28 SBA-15, Zn-SBA-15 and Zn-PADO-HMDS-SBA-15 catalysts produced poly(ϵ -
29 caprolactone) with a narrow molecular weight distribution, close to one. In all cases
30 polymerization was confirmed to proceed via a coordination insertion mechanism after
31 end group analysis by ¹H NMR.

32

33 **Keywords:** ring opening polymerization, heterogeneous catalyst, SBA-15, titanium,
34 zinc, aluminium, magnesium.

35 Introduction

36

37 Conventional plastics possess excellent properties. However, the high durability of
38 these synthetic polymers has caused a crisis in solid waste management. New
39 regulations affecting packaging producers will force them to take charge of their waste
40 in the future.¹ In response industry and scientific community have enhanced the
41 research in new materials compatible with the environment. Biodegradable polymers,
42 poly(caprolactone) (PCL), polyglycolide (PGA), polylactide (PLA) and their
43 copolymers, besides their bulk applications in packaging and various other consumer
44 goods are particular interesting in medicine and tissue engineering purposes due to their
45 biocompatibility. Especially, interest toward polycaprolactone (PCL) homopolymer for
46 medical devices has extensively increased ever since it was discovered that it is suitable
47 scaffold material for cells in repairing and regenerating tissue defects and as a drug
48 delivery agent.^{2,3} The biodegradability of poly(ϵ -caprolactone)⁴ and its copolymers with
49 available renewable resources (lactide or glycolide)^{5,6} has made it a preferred choice
50 for potential environmentally friendly commodity plastic and the demand for this
51 polymer is ever increasing.

52

53 An upcoming challenge is to produce biodegradable polymers or copolymers based
54 on poly(ϵ -caprolactone) at low cost and with physical properties that would make them
55 industrial competitors to non-biodegradable, well established commodity polymers such
56 as poly(ethylene). These polyesters are most commonly produced by ring opening
57 polymerizations (ROPs) of the cyclic esters using cationic, anionic and coordination–
58 insertion polymerization techniques.⁷ The latter has received significant interest as it
59 offers an efficient method to control molecular weight and molecular weight
60 distribution of the polyesters and thus, these properties of polyesters can be modified
61 with great precision.

62

63 Homogeneous catalysts have been designed that can control polymer molecular
64 weights, molecular weight distributions, co-monomer incorporation and
65 stereochemistry. Typical single site catalysts for lactone polymerization are of the form
66 $M(OR)L_n$, where the alkoxy group (OR) is capable of propagation. These complexes are
67 conceptually different from typical lactone polymerization catalysts of the form

68 $M(OR)_n$, which do not possess a permanent ancillary ligand.⁸ A large variety of new
69 single site catalytic systems based on tin,⁹ aluminium,^{10,11} zinc,¹² magnesium,¹³ iron,¹⁴
70 lanthanide,¹⁵ titanium¹⁶ and lithium¹⁷ organometallic complexes containing initiating
71 groups such as amides, carboxylates, and alkoxides have been reported.^{18, 19}

72

73 From a practical point of view, it would be desirable for these catalysts to be
74 heterogeneous to allow for better control of the polymerization process and easier
75 separation of the catalysts from the polymer product and some examples have been
76 reported in recent years of immobilization of metallic precursors on inorganic supports.
77 Homoleptic alkoxy complexes, such as titanium and calcium alkoxy complexes have
78 been supported on silica substrates by Chung²⁰ and George,²¹ respectively; to prepare
79 catalysts active in polymerization of L-lactide and ϵ -caprolactone (ϵ -CL). Previously,
80 Jeromé has supported [Tris(hexamethyldisilyl)amide]yttrium on silica to use this
81 material as initiator in the ROP of ϵ -CL in the presence of 2-propanol²² and Spitz et al.
82 have published the synthesis of silica grafted lanthanide amide and its transformation
83 into an alkoxide, testing this new material in the ROP of ϵ -CL in the presence of benzyl
84 alcohol.²³

85

86 Single site catalysts have been also used as useful precursors. C.W. Jones et al. have
87 anchored β -Diiminate zinc alkoxy complexes onto SBA-15 for polymerization of
88 lactide.²⁴ Recently, M. D. Jones and co-workers have published the tethering of zinc²⁵
89 and aluminium Schiff bases onto silica and their behaviour as catalysts in the
90 polymerization of *rac*-lactide.²⁶

91

92 A different approach has been the choice of alternative supports. C.W. Jones et al.
93 have published the preparation of magnetic nanoparticles supported aluminium
94 isopropoxy as a new catalyst for the ring-opening polymerization of ϵ -CL.²⁷
95 Tantirungrotechai and co-workers have successfully used aluminium and calcium-
96 incorporated MCM-41-type silica as catalytic supports for the polymerization of L-
97 lactide and ϵ -CL, the catalytic centres were generated by grafting titanium(IV)
98 isopropoxide onto the support.²⁸

99

100 Among the inert supports used in the last decade, for the heterogenization of
101 catalytically active species, well ordered mesoporous silica are without doubt one of the
102 most promising family of materials. The support used in the present study SBA-15 has
103 become the most popular member of the highly ordered mesoporous (20-300 Å) silica
104 structure family synthesized by the use of commercially available poly(alkylene oxide)
105 triblock copolymer surfactant species. SBA-15 has a two-dimensional $p6mm$ hexagonal
106 structure, with a well ordered hexagonal array and one-dimensional channel structure. It
107 possesses high thermal stability, very high surface areas ($>800 \text{ m}^2\text{g}^{-1}$), pores large
108 enough (8 to 11 nm) to immobilize molecular catalysts (e.g. metal complexes) and
109 uniformly sized and shaped tunable pores have the potential to induce shape selectivity
110 in the local environment of the active centre. Another important aspect of SBA-15
111 materials is linked to the commercial requirements for their synthesis. There is a strong
112 demand for low cost processes, the possibility of scaling-up the batch size, high yields
113 and synthesis efficiency.²⁹

114

115 In this study, new mesoporous heterogeneous catalysts have been prepared by
116 different strategies. The post grafting process through covalent linkage of surface silanol
117 groups and active titanium, aluminium, magnesium and zinc precursors has been
118 regarded as an alternative route for the preparation of metal ion doped mesoporous
119 materials. This process avoids the introduction of heteroatoms into the framework of the
120 ordered mesostructures and the catalytically active centres are located at the pore
121 surface, which are easily accessible to the reactants. However, the formation of
122 oligomeric species make the immobilization of active groups onto the support through
123 coordination of metal to a terminal functional group of a surface bound linker, based on
124 an amino alcohol chelate ligand, a good alternative that ensures the purity of pseudo-
125 homogeneous complex present on the support. The catalytic performance of the
126 prepared materials has been studied in the ring opening polymerization of ϵ -CL and
127 compared with their homogenous counterparts.

128

129

130 **Experimental section**

131 **General procedures**

132 All reactions were performed using standard Schlenk tube techniques under an
133 atmosphere of dry nitrogen or argon. Tetraethylortosilicate (TEOS) 98% ($M = 208.33$, $d =$
134 0.934 g mL^{-1}), poly(ethylene glycol)-block-poly(propylene glycol)-block-
135 poly(ethylene glycol) ($M_{av} = 5800$, $d = 1.007 \text{ g mL}^{-1}$), hexamethyldisilazane (HMDS)
136 ($M = 161.39$, $d = 0.774 \text{ g mL}^{-1}$), dimethyl zinc (ZnMe_2) 2 M in toluene, 3-[Bis(2-
137 hydroxyethyl)amino]propyl-triethoxysilane] solution 65% in ethanol ($M = 309.47$ $d =$
138 0.94 g mL^{-1}), di-n-butylmagnesium ($\text{Mg}(\text{}^n\text{Bu})_2$) 1 M in heptane ($M = 138.53$ $d = 0.713 \text{ g}$
139 mL^{-1}), methyl aluminium (AlMe_3) 2 M in toluene ($M = 72.09$ $d = 0.752 \text{ g mL}^{-1}$) and
140 aluminium isopropoxide ($\text{Al}(\text{O}^i\text{Pr})_3$) ($M = 204.24$), were purchased from Sigma Aldrich
141 and used as received. Titanium tetraisopropoxide 97% ($\text{Ti}(\text{O}^i\text{Pr})_4$) ($M = 284.22$, $d =$
142 0.955 g mL^{-1}) were purchased from Sigma Aldrich distilled and stored under a nitrogen
143 atmosphere prior to use. ϵ -caprolactone ($M = 114.14$, $d = 1.003 \text{ g mL}^{-1}$) was purchased
144 from Fluka, and was refluxed over CaH_2 , distilled and stored under a nitrogen
145 atmosphere prior to use. Hydrochloric acid 35% was purchased from Panreac. Organic
146 solvents were purchased from SDS and distilled and dried before use according to
147 conventional literature methods. Water was obtained from a Millipore Milli-Q system
148 (Waters, USA). The hexagonal material (SBA-15) was prepared using a poly (alkaline
149 oxide) triblock copolymer surfactant in an acidic medium, according to the method of
150 *Zhao et al.* Silica was purchased from Sigma Aldrich. Homogeneous titanium and zinc
151 catalysts designated as Ti-PADO and Zn-PADO have been synthesized according to
152 previously published procedures³⁰.

153

154 **Characterization**

155 X-ray diffraction (XRD) patterns of the silicas were obtained on a Phillips
156 Diffractometer model PW3040/00 X'Pert MPD/MRD at 45 KV and 40 mA, using Cu-
157 $K\alpha$ radiation ($\lambda = 1.5418 \text{ \AA}$). N_2 gas adsorption-desorption isotherms were obtained
158 using a Micromeritics TriStar 3000 analyzer, and pore size distributions were calculated
159 using the Barret-Joyner-Halenda (BJH) model on the adsorption branch. Infrared
160 spectra were recorded on a Nicolet-550 FT-IR spectrophotometer (in the region 4000 to
161 400 cm^{-1}) as nujol mulls between polyethylene pellets and KBr disks. Proton-
162 decoupled ^{29}Si MAS NMR spectra were recorded on a Varian-Infinity Plus 400 MHz

163 Spectrometer operating at 79.44 MHz proton frequency (4 μ s 90° pulse, 1024 transients,
164 spinning speed of 5 MHz). Cross Polarization ^{13}C CP/MAS NMR spectra were recorded
165 on a Varian-Infinity Plus 400 MHz Spectrometer operating at 100.52 MHz proton
166 frequency (4 μ s 90° pulse, 4000 transients, spinning speed of 6 MHz, contact time 3 ms,
167 pulse delay 1.5 s). Elemental analysis (% C and % N) was performed by the
168 Investigation Service of Universidad de Alcalá (Spain) using a CHNS analyser LECO-
169 932 model. The titanium, aluminium, magnesium and zinc content was determined by
170 XRF Scanning electron micrographs and morphological analysis were carried out on a
171 XL30 ESEM Philips. The DR UV-Vis spectroscopic measurements were carried out on
172 a Varian Cary-500 spectrophotometer equipped with an integrating sphere and
173 polytetrafluoroethylene (PTFE) as reference, with $d = 1\text{ g cm}^{-3}$ and thickness of 6 mm.
174 The electronic absorption UV-vis spectra were recorded in toluene solution on a UV-
175 Vis Analytik Jena Specord 200PC spectrophotometer. Thermogravimetric analysis was
176 performed using a Setsys 18 A (Setaram) thermogravimetric analyzer.

177

178 **Synthesis**

179 **Synthesis of homogeneous Al and Mg complexes**

180 An equimolar amount of AlMe_3 , 2 M in toluene (1.00 mL, 2.0 mmol) was added to a
181 toluene solution (25 mL) of 3-[Bis(2-hydroxyethyl)amino]propyl-triethoxysilane] 65%
182 in ethanol (1.06 mL, 2.0 mmol) at 0°C. The reaction evolves with methane elimination
183 as temperature increases to room temperature. The solution was stirred for 4 h,
184 afterwards the solvent was removed in vacuo, and the resulting solid washed with
185 hexane (2 \times 10 mL) to give complex Al(Me)-PADO as a white solid. In a similar way
186 complexes Al-PADO and Mg-PADO have been prepared by using equimolar amounts
187 of $\text{Al}(\text{O}^i\text{Pr})_3$ (0.2 g, 2.0 mmol) and $\text{Mg}(\text{}^n\text{Bu})_2$ (1.00 mL, 2 mmol) toluene solutions to get
188 white solids sparingly soluble in toluene.

189

190 **Synthesis of heterogeneous catalyst**

191 *Grafting of $\text{Ti}(\text{O}^i\text{Pr})_4$, ZnMe_2 , $\text{Mg}(\text{}^n\text{Bu})_2$ or $\text{Al}(\text{O}^i\text{Pr})_3$ onto SBA-15*

192 1 g of SBA-15 previously dehydrated at 150 °C during 15 h was suspended in 50
193 mL of dry toluene, and to the mechanically stirred suspension $\text{Ti}(\text{O}^i\text{Pr})_4$ (1.2 mL, 4
194 mmol), ZnMe_2 (2.0 mL, 4 mmol) or $\text{Mg}(\text{}^n\text{Bu})_2$ (4.8 mL, 4 mmol), was added by syringe.
195 $\text{Al}(\text{O}^i\text{Pr})_3$ (0.8 g, 4 mmol) was previously dissolved in 10 mL of dry toluene and transfer

196 to the SBA-15 suspension. In all cases the reactant mixture was stirred at room
197 temperature for 24 h. The solid was filtered off, washed repeatedly with toluene and
198 hexane, dried under vacuum and stored under inert atmosphere. The obtained materials
199 have been labelled as Ti-SBA-15, Zn-SBA-15, Mg-SBA-15 and Al-SBA-15,
200 respectively.

201

202 *Functionalization of SBA-15 with 3-[Bis(2-hydroxyethyl)amino]propyl-*
203 *triethoxysilane] in the presence of hexamethyldisilazane as capped agent.*

204 In a typical experiment 1 g of SBA-15 silica was suspended in 30 mL of dry
205 toluene, hexamethyldisilazane (HMDS) (0.84 mL, 4 mmol) and 3-[Bis(2-
206 hydroxyethyl)amino]propyl-triethoxysilane] in ethanol solution (2 mL, 4 mmol) were
207 added in turn. The reactan mixture was stirred for 24 h at 90 °C and the resulting solid
208 labelled with the acronym of PADO-HMDS-SBA-15, was filtered off and washed with
209 toluene (2 × 50 mL) and hexane (1 × 50 mL). The final material was dried under
210 vacuum and stored under inert atmosphere.

211

212 *Tethering of $Ti(O^iPr)_4$, $ZnMe_2$, $AlMe_3$, $Al(O^iPr)_3$ or $Mg(^nBu)_2$ onto PADO-HMDS-*
213 *SBA-15.*

214 1 g of PADO-HMDS-SBA-15 was dissolved in dry toluene (45 mL) and reacted
215 with an excess of $Ti(O^iPr)_4$, $ZnMe_2$, $AlMe_3$, $Al(O^iPr)_3$ or $Mg(^nBu)_2$, (4 mmol),
216 respectively. The reaction mixture was stirred at room temperature for 24 h and the final
217 product collected by filtration and washed with dry toluene (2 × 50 mL) and with
218 hexane (1 × 50 mL). The obtained materials, designated as Ti-PADO-HMDS-SBA-15,
219 Zn-PADO-HMDS-SBA-15, Al(Me)-PADO-HMDS-SBA-15, Al-PADO-HMDS-SBA-
220 15 and Mg-PADO-HMDS-SBA-15, were dried under vacuum and stored under inert
221 atmosphere.

222

223 **ϵ -caprolactone polymerization**

224 Polymerization of ϵ -caprolactone was carried out under inert atmosphere using a
225 flask equipped with a magnetic stirrer. Predetermined amounts of purified ϵ -CL, dried
226 toluene, and homogeneous or heterogeneous catalyst were charged and the monomer was
227 added by syringe with vigorous magnetic stirring. The polymerization studies were
228 carried out at room temperature and 80 °C, for homogenous catalysts and heterogeneous

229 catalysts, respectively. In kinetic or mechanism studies in homogeneous phase small
230 aliquots were taken at different reactions times depending on the catalyst (See results and
231 discussion section). After the reaction time had elapsed the ϵ -CL polymerization was
232 quenched by addition of 5 mL of methanol, the solid phase was separated by filtration
233 and the polymer precipitated with an excess of methanol. The polymer was washed with
234 methanol and dried at 50 °C under vacuum for 12 h. The sample was subjected to ^1H
235 NMR spectroscopy (CDCl_3) and gel permeation chromatography (GPC) to determine the
236 average molecular weights M_n , M_w of the produced polymer and molecular weight
237 distribution (PDI). The monomer conversion was determined from the relative intensity
238 of the NMR signals at δ 4.20 and 4.02 ppm corresponding to the OCH_2 resonance in ϵ -
239 caprolactone and poly(ϵ -caprolactone), respectively.

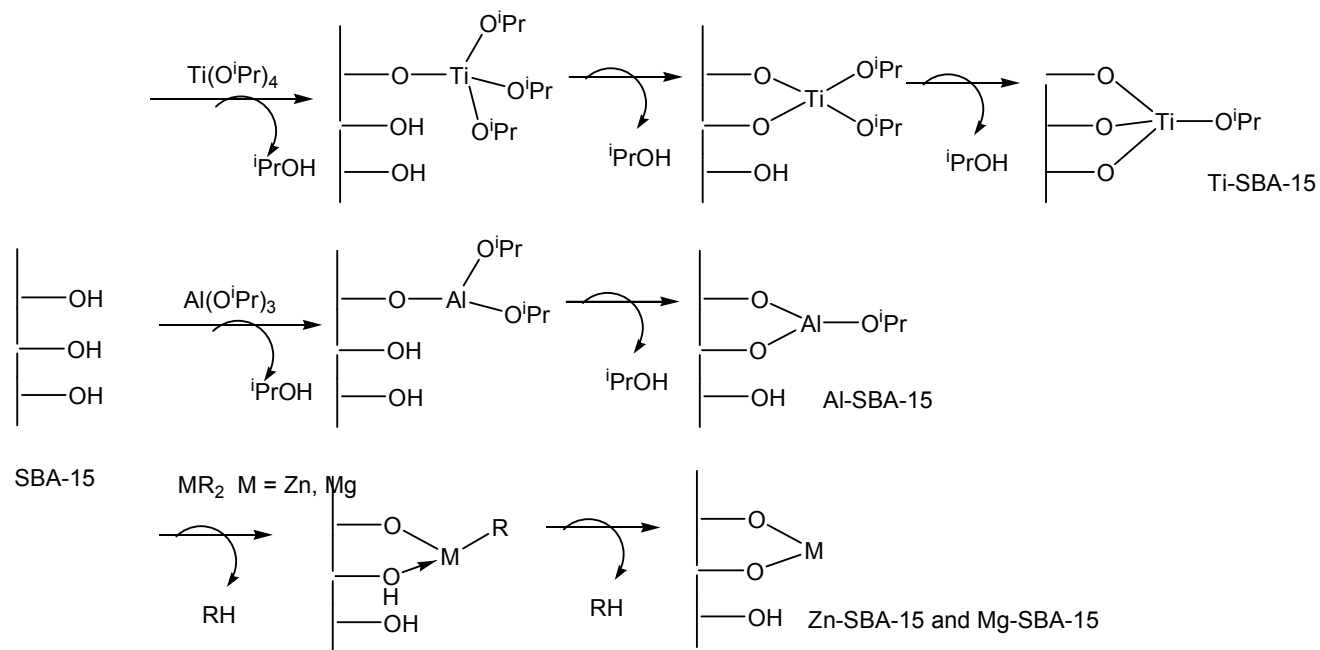
240 Results and discussion

241 Synthesis of titanium, zinc, aluminium and magnesium mesoporous M-SBA-15 and 242 analogous metallic hybrid M-PADO-HMDS-SBA-15 materials.

243 The materials Ti-SBA-15, Zn-SBA-15, Al-SBA-15 and Mg-SBA-15 have been
244 prepared by direct reaction of 1g of SBA-15 mesoporous silica, previously dehydrated,
245 with 4 mmol of $\text{Ti}(\text{O}^i\text{Pr})_4$, ZnMe_2 , $\text{Al}(\text{O}^i\text{Pr})_3$ or $\text{Mg}(\text{}^n\text{Bu})_2$ in toluene under an inert
246 atmosphere for 24 h (Scheme 1). This process avoids the introduction of heteroatoms
247 into the framework of the ordered mesostructure and guarantees that the chemically
248 active metallic centres are located at the pore surfaces of the parent SBA-15.

249
250 Alternatively, an organic-inorganic hybrid SBA-15 material has been synthesized
251 slightly modifying published procedures.^{31,32} The material with the acronym PADOH-
252 HMDS-SBA-15 has been prepared by one step reaction of dehydrated SBA-15 with a
253 mixture of silylating agents, an alkoxy silane compound; 3-[bis(2-
254 hydroxyethyl)amino]propyl-triethoxysilane] (PADOH) and the silylamine,
255 hexamethyldisilazane (HMDS), a capped agent capable of masking the remaining silanol
256 groups available in the silica surface and of increasing surface hydrophobicity. In the
257 second stage titanium, zinc, aluminium and magnesium materials have been obtained by
258 tethering the corresponding alkoxy or alkyl metallic precursor onto organomodified or
259 PADOH-HMDS-SBA-15 (Scheme 2). The immobilization of active groups onto the
260 silica support through coordination of metal to a covalently bonded linker based on an

- 261 amino alcohol chelate ligand should ensure the purity of pseudo-homogeneous single
262 site complexes present on the support.

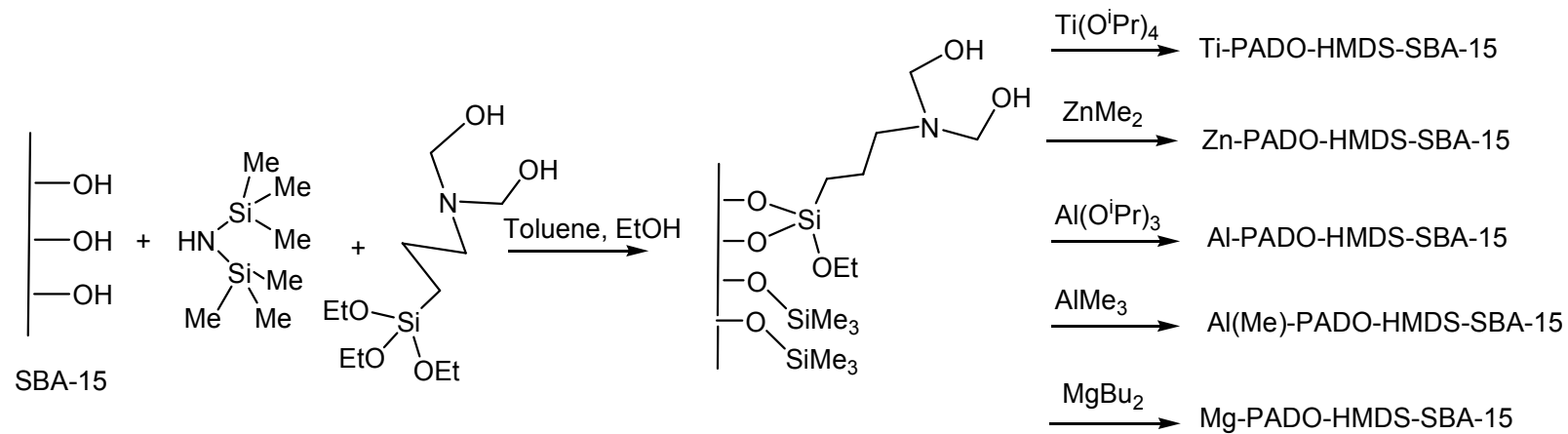


Scheme 1. Preparation of Ti-SBA-15, Zn-SBA-15, Al-SBA-15 and Mg-SBA-15 materials.

263

264

265



266

267

268

269 Scheme 2. Preparation of Ti-PADO-HMDS-SBA-15, Zn-PADO-HMDS-SBA-15, Al-PADO-HMDS-SBA-15, Al(Me)-PADO-HMDS-SBA-15

270 and Mg-PADO-HMDS-SBA-15 materials

271

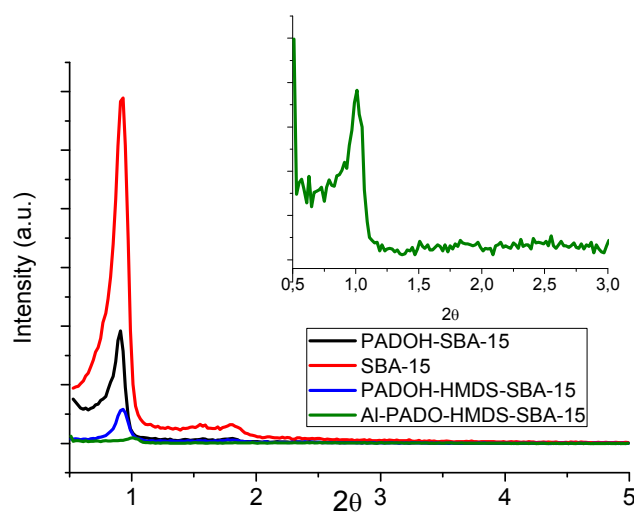
272

273 **Characterization of titanium, zinc, aluminium and magnesium mesoporous SBA-**
274 **15 and Hybrid PADO-HMDS-SBA-15 Materials**

275

276 XRD patterns of the organic inorganic hybrid material are similar to those of the
277 corresponding parent support, revealing the (100) reflection peak at $2\theta \cong 0.92$
278 characteristic of the hexagonally ordered arrangement of SBA-15 (Fig. 1). d-Spacing
279 value for this XRD peak is 96.02 Å and a_0 is equal to 110.88 Å. The results confirm that
280 the ordered mesoporous structure of SBA-15 remains intact after the functionalization
281 procedure with PADOH or the mixture PADOH/HMDS. An overall decrease in
282 intensity is observed which can be attributed to the lowering local order, such as
283 variations in the wall thickness of the framework or reduction of scattering contrast
284 between the channel wall and the ligands present on the inner surface of SBA-15 (Table
285 1). As an example, similar behaviour is observed by studying the diffractograms of Al-
286 PADO-HMDS-SBA-15; compared to parent SBA-15 the aluminium tethered sample
287 shows an important decrease in the relative intensities of the XRD.

288



289

290 Fig. 1. XRD patterns of SBA-15; PADOH-SBA-15, PADOH-HMDS-SBA-15 and Al-
291 PADO-HMDS-SBA-15.

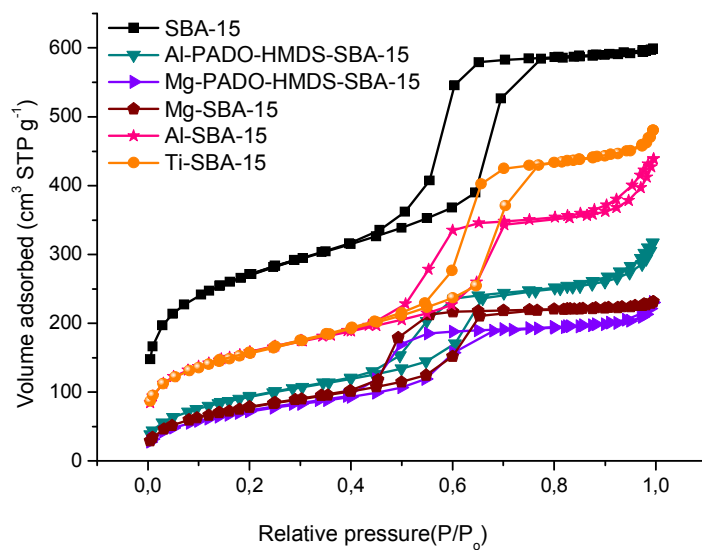
292 The N_2 adsorption–desorption isotherms of hybrid materials can be classified as
293 type IV characteristic of mesoporous materials (Fig. 2, Fig. S1 and S2). The mesopores
294 are uniform in size, which is indicated by the sharp increase in N_2 uptake for adsorption,
295 observed at P/P_0 ca. 0.50–0.70. After silylation and aminediol ligand incorporation a

296 drastic decrease in the S_{BET} , pore volume and average BJH pore diameter were observed
297 (see Table 1), changes that can be interpreted as being due to the presence of organic
298 molecules anchored to the channels partially blocking the adsorption of nitrogen
299 molecules. Since most of the aminediol sites which can bind with active metal centres in
300 PADOH-HMDS-SBA-15, are located at the surface, it is clearly seen that surface area
301 and pore volume gradually decrease with subsequent complexation with metal ions.
302 Thus, we can conclude that the organic moiety, as well as, the metal ions are grafted
303 inside the mesopore cavity.

304 The nitrogen content obtained from elemental analysis for PADOH-SBA-15 and
305 PADOH-HMDS-SBA-15 was 1.44% and 0.94%, respectively (Table 2). The aminediol
306 based ligand loading was found to be 1.03 and 0.67 mmol g^{-1} . Taking into account these
307 values and S_{BET} of the parent mesoporous silica, the average surface density (d ,
308 molecules nm^{-2}) of the attached molecules and the average intermolecular distance (l ,
309 nm) were calculated. The values obtained were $d = 0.70$ and $l = 1.20$ nm for PADOH-
310 SBA-15 and $d = 0.46$ and $l = 1.48$ nm for PADOH-HMDS-SBA-15. On the basis of
311 carbon and nitrogen content measurements the amount of capped ligand was also
312 calculated for PADOH-HMDS-SBA-15 using the following expression: mmol capped
313 agent/g = mmolC/g-(mmolN/g \times nC), being nC = number of carbon atoms in PADOH
314 and assuming total condensation, three surface silanol groups react with three ethoxy
315 groups ($-\text{OC}_2\text{H}_5$). The obtained value 8.04 mmol HMDS/g suggests that under the
316 prevailing experimental conditions the competitive silylation reaction achieved a higher
317 $-\text{SiMe}_3$ surface coverage.

318 The metal loading was calculated by X-ray fluorescence (XRF). Considering that
319 the hybrid organic-inorganic materials metal complexes are anchored via the
320 incorporated ligand into the mesoporous silica, the anchoring efficiency of metal toward
321 the linker can be estimated taking into account the amount of incorporated ligand and
322 metal loading. The measured metal content for Ti and Zn-PADOH-HMDS-SBA-15 is
323 4.14 and 2.04 %, respectively, which corresponds to 0.86 and 0.84 mmol g^{-1} . These data
324 show a molar ratio or metal: ligand ratio near to one which suggests the formation of
325 titanium and magnesium complexes with 1:1 stoichiometry. The ratio metal to ligand
326 obtained for zinc hybrid mesoporous materials increases significantly, supporting a
327 better anchored efficiency and the formation of complexes with 1:2 stoichiometry. In

328 the case of aluminium the immobilization efficiency is slightly higher for AlMe_3 in
329 comparison to $\text{Al}(\text{O}^i\text{Pr})_3$, yielding anchored complexes with 1:1 stoichiometry (See
330 table 1).



331

332 Fig. 2. Nitrogen adsorption-desorption isotherms profiles of Mg-SBA-15; Al-SBA-15,
333 Mg-PADO-HMDS-SBA-15 and Al-PADO-HMDS-SBA-15.

334 **Table 1.** Textural properties and metal content of the mesoporous SBA-15 materials

Material	S_{BET} ($\text{m}^2 \text{g}^{-1}$)	Pore Volume ($\text{cm}^3 \text{g}^{-1}$)	Pore size (\AA)	Metal content ^a (%)	Metal content ^a (mmol g^{-1})
SBA-15	886	1.03	57	-	
PADOH-SBA-15	463	0.56	55	-	
PADOH-HMDS-SBA-15	390	0.50	54	-	
Ti-SBA-15	557	0.70	51	15.50	3.24
Zn-SBA-15	626	0.95	55	12.80	1.96
Al-SBA-15	610	0.81	53	6.89	2.55
Mg-SBA-15	292	0.35	48	4.85	2.00
Zn-PADO-HMDS-SBA-15	311	0.40	51	9.42	1.44
Al-PADO-HMDS-SBA-15	352	0.44	52	2.56	0.95
Al(Me)-PADO-HMDS-SBA-15	292	0.44	53	2.91	1.08
Mg-PADO-HMDS-SBA-15	270	0.32	48	2.04	0.84
Zn-PADO-HMDS-Silica	194	0.32	65	12.50	1.91

335 ^a Metal content calculated by X-ray fluorescence (XRF)

336 **Table 2.** C and N contents (wt.%) obtained by elemental chemical analysis (CNH)

Material	%N	%C	mmol N g ⁻¹	mmolC g ⁻¹	mmol Ligand g ⁻¹ ^a	mmol capped agent g ⁻¹ ^b	Surface coverage (number of PADOH/PTDO H per nm ²) ^c	Capped agent/Ligand ratio
PADOH-SBA-15	1.44	14.55	1.03	12.13	1.03		0.70	
PADOH-HMDS-SBA-15	0.94	13.68	0.67	11.40	0.67	8.04	0.46	11.98

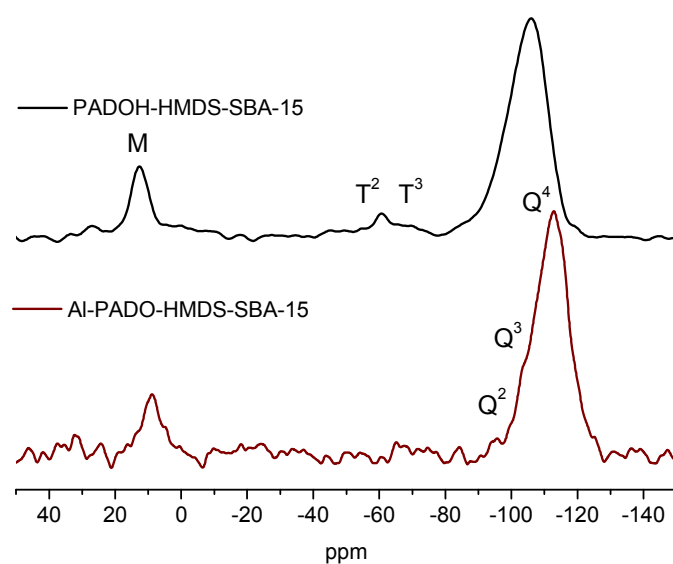
337 ^a mmol Ligand g⁻¹, calculation from mmol N g⁻¹ values since PADOH ligands possesses one nitrogen atoms in its structure.

338 ^b mmol capped agent (hexamethyldisilazane) g⁻¹, calculation from C mmol g⁻¹ values. mmol capped agent g⁻¹ = C mmol g⁻¹-(N mmol g⁻¹×nC),
 339 being nC = number of carbon atoms in PADOH ligand assuming total condensation, three surface silanol groups react with three ethoxy groups
 340 (-OC₂H₅)

341 ^c Surface coverage: Example: $\alpha(\text{PADOH}) = \delta(\text{PADOH})N_A a_s^{-1} \times 10^{-18}$ (number of PADOH groups per nm²) being $\delta(\text{PADOH}) = \%N(100n_N M_N)^{-1}$
 342 [mol g⁻¹] = concentration of surface PADOH groups, %N = wt% referred to the parent SBA-15 silica; N_A = Avogadro constant (6.022×10²³ mol⁻¹);
 343 a_s = specific BET surface area of dehydrated, non modified SBA-15 (886 m² g⁻¹); n_N = number of nitrogen atoms per PADOH group (-N-
 344 ((CH₂-OH)₂, 1); M_C = atomic weight of nitrogen (14.010 g mol⁻¹).

345 .

346 The hybrid materials were also characterized by ^{29}Si and ^{13}C MAS NMR. As an
347 example, ^{29}Si MAS NMR spectra of PADOH-HMDS-SBA-15 and Al-PADO-HMDS-
348 SBA-15 are shown in Fig. 3. The spectra of the functionalized silica shows two main
349 peaks at -110 and -101 ppm assigned to Q^4 framework silica sites ($(\text{SiO})_4\text{Si}$) and Q^3
350 silanol sites ($(\text{SiO})_3\text{SiOH}$), respectively. A marked decrease in the intensity of the Q^3
351 signal in comparison with parent SBA-15 is observed, which verified the tethering of
352 the functional groups to Si-OH. T^2 ($\text{RSi}(\text{OSi})_2(\text{OR}')$) and T^3 ($\text{RSi}(\text{OSi})_3$) organosilane
353 species at -57 and -63 ppm, respectively, present in the functionalized material are
354 indicative of a high degree of condensation of the triethoxysilanes with the silica
355 surface. In addition, the choice of HMDS as protecting group allows an easy
356 determination of the trimethylsilyl groups by ^{29}Si NMR; the new peak of the silylating
357 agent, an M site ($(\text{Me}_3\text{SiO}-)$), is seen at 12 ppm.

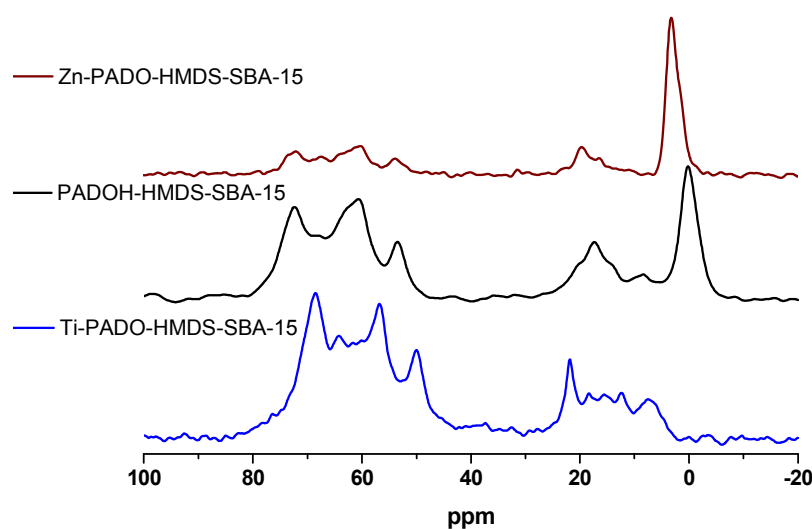


358

359 Fig. 3. ^{29}Si MAS NMR spectrum of PADOH-HMDS-SBA-15 and Al-PADO-HMDS-
360 SBA-15.

361 ^{13}C CP MAS NMR studies provide useful information regarding the presence of
362 organic moiety and the chemical interaction of metal ions with the donor sites in the
363 hybrid frameworks. In Fig. 4 the ^{13}C CP MAS NMR spectra of metal containing
364 materials are shown in comparison to the parent PADOH-HMDS-SBA-15. The
365 spectrum for the metal free aminediol ligand containing mesoporous material exhibits
366 three signals from the three carbon atoms present in the alkyl chain at 7, 16 and 58 ppm

367 for $\equiv\text{Si}-\text{CH}_2-$, $\text{CH}_2-\text{CH}_2-\text{CH}_2-$ and $-\text{CH}_2-\text{O}$, respectively. In addition two additional
 368 signals at 16 and 50 ppm attributed to the unreacted ethoxy groups attached to Si in the
 369 aminediol silane ligand are observed. The signal attributed to methylenic carbons $-\text{N}-$
 370 $(\text{CH}_2-\text{OH})_2$ of aminediol ligand appears at 69 ppm. As characteristics signals in Ti-
 371 PADO-HMDS-SBA-15 it is worth mentioning the signals of the isopropoxy ligand at
 372 21 and 64 ppm for methyl $(\text{CH}_3)_2-\text{CH}-\text{O}$ and methyne $(\text{CH}_3)_2-\text{CH}-\text{O}$ groups,
 373 respectively. The spectrum of Zn-PADO-HMDS-SBA-15 shows an identical pattern to
 374 that of the parent material.

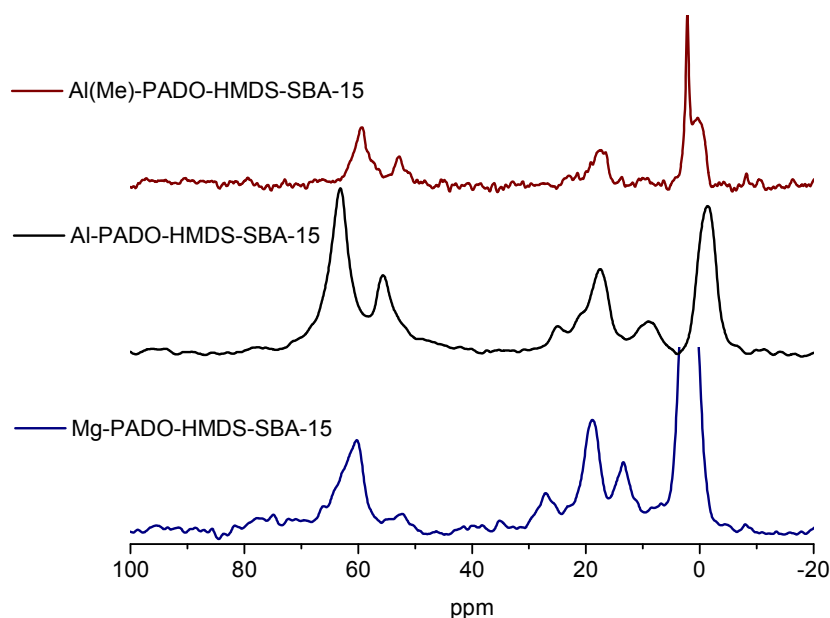


375

376 Fig. 4. ^{13}C MAS NMR spectra of Zn-PADO-HMDS-SBA-15, PADOH-HMDS-SBA-15
 377 and Ti-PADO-HMDS-SBA-15 materials.

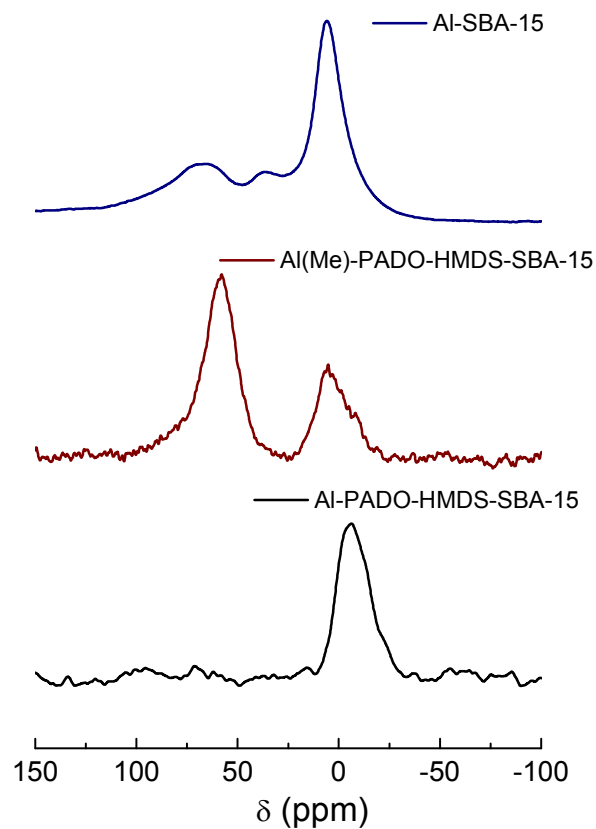
378 In order to obtain extra information about the possible structure of the catalyst, two
 379 aluminium precursors have been anchored on the aminediol based SBA-15 material.
 380 Fig. 5 shows the ^{13}C CP MAS NMR spectra of both materials that confirm the presence
 381 of different aluminium complexes immobilized on the silica surface depending on the
 382 metal precursor. As significant signals the spectrum of the material synthesized by using
 383 AlMe_3 shows a sharp signal at 2 ppm attributed to the methyl group directly bonded to
 384 aluminium, meanwhile the spectrum of the material synthesized by using $\text{Al}(\text{O}^i\text{Pr})_3$
 385 shows at 21 ppm the characteristic signal of the methyl groups $(\text{CH}_3)_2-\text{CH}-\text{O}$ in the
 386 isopropoxy ligand. ^{27}Al solid state NMR spectroscopy is a good tool for the
 387 determination of the aluminium coordination number in complexes. It is well known

388 that ^{27}Al solid state NMR spectra show a signal between -10 and +20 ppm for
389 coordination number six and between +55 and +85 ppm for coordination number four.
390 Some rare examples of five-coordinate aluminium are known, with signals near +35
391 ppm. Fig. 6 shows the ^{27}Al NMR CP NMR spectra of Al(Me)-PADO-HMDS-SBA-15
392 and Al-PADO-HMDS-SBA-15; two signals at 58 and 5 ppm are observed for the first
393 material, which clearly indicates the presence of aluminium centres with different
394 coordination environments, four and six, respectively when the metallic precursor
395 employed in the immobilization procedure is AlMe_3 . If $\text{Al}(\text{O}^i\text{Pr})_3$ is used instead, the
396 aluminium atoms are probably octahedrally coordinated as made evident by the
397 presence of only one signal at -6 ppm.³³ Finally, in the ^{27}Al NMR spectrum of Al-
398 SBA-15 three resonances are observed at 6, 37 and 66 ppm, for tetrahedral, 5 coordinate
399 and octahedral aluminium environments. Taking into account the experimental results,
400 the proposed structures for the materials synthesized using two different aluminium
401 precursors are shown in Fig. 7a and 7b.



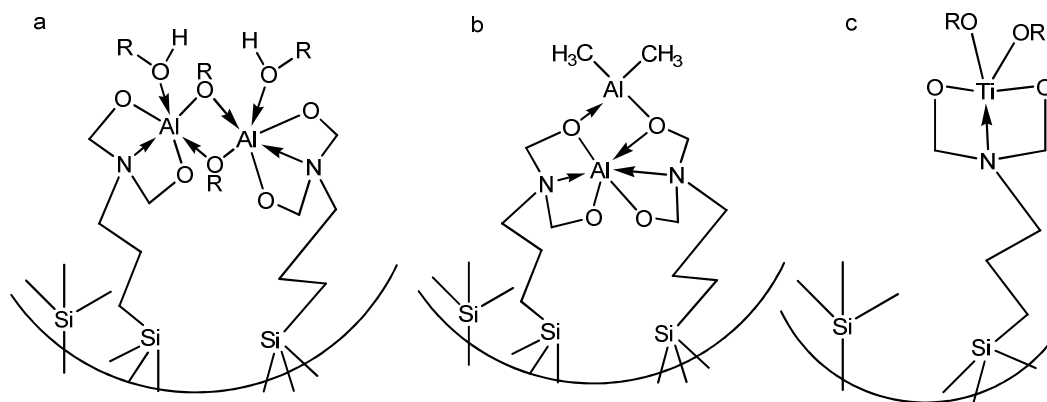
402

403 Fig. 5. ^{13}C CP MAS NMR spectra of Al(Me)-PADO-HMDS-SBA-15, Al-PADO-
404 HMDS-SBA-15 and Mg PADO-HMDS-SBA-15 materials.



405

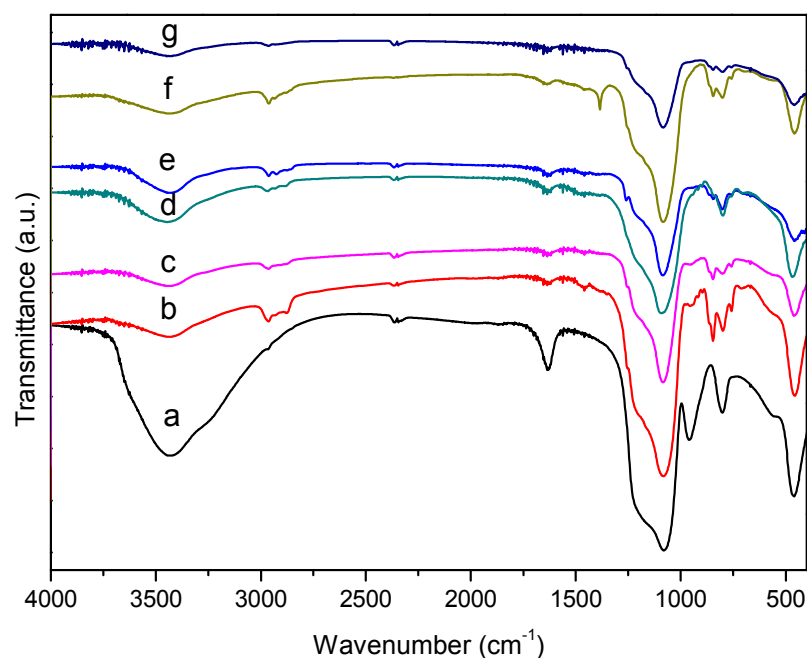
406 Fig. 6. ^{27}Al CP MAS NMR spectra of Al-SBA-15, Al(Me)-PADO-HMDS-SBA-15 and
407 Al-PADO-HMDS-SBA-15.

408
409

410 Fig. 7. Proposed structure for the different materials a) Al-PADO-HMDS-SBA-15, b)
411 Al(Me)-PADO-HMDS-SBA-15 and c) Ti-PADO-HMDS-SBA-15.

412 FT-IR spectra of mesoporous SBA-15 silica heterogenized aminediol ligand with
413 and without the presence of capped trimethylsilyl groups have been recorded before and
414 after metal immobilization; as well as, FT-IR spectra of parent SBA-15 before and after
415 metal immobilization between 4000-400 cm^{-1} (Fig. 8 and Fig. 9). The main features of
416 the SBA-15 spectra include a large broad band between 3400 and 3200 cm^{-1} , which is
417 attributed to O-H stretching of the surface silanol groups and the remaining adsorbed
418 water molecules. The siloxane (-Si-O-Si-) band appears as a broad strong peak centred
419 at 1100 cm^{-1} . The band due to Si-O bond stretching of the silanol groups was observed
420 at 960 cm^{-1} . The adsorption band at 1630 cm^{-1} is due to deformation vibrations of
421 adsorbed water molecules.³⁴ After functionalization with 3-[Bis(2-
422 hydroxyethyl)amino]propyl-triethoxysilane] the absorption peak of the Si-OH groups
423 and physisorbed water decrease, new bands appear in the range 2873-2964 attributed to
424 the $\nu(\text{C-H})$ stretching vibrations, at 1459 and 1353 cm^{-1} and in the range 764-843 cm^{-1}
425 assigned to the γ (-CH₂-) alkyl chain due to the anchored ligand (Fig. S3). After the one
426 pot reaction with the equimolar mixture of 3-[Bis(2-hydroxyethyl)amino]propyl-
427 triethoxysilane] and hexamethyldisilazane a similar pattern is observed with addition of
428 HMDS a strong band at 798 cm^{-1} γ (-CH₃) belonging to the Me₃Si-O-Si≡ groups on the
429 silica surface (Fig. S3). Fig. 8 and Fig. S4 show some of the above mentioned spectra
430 and those obtained upon metal immobilization. As can be seen the formation of the
431 anchored complexes on the silica surface does not modify the FT-IR spectra
432 significantly.

433

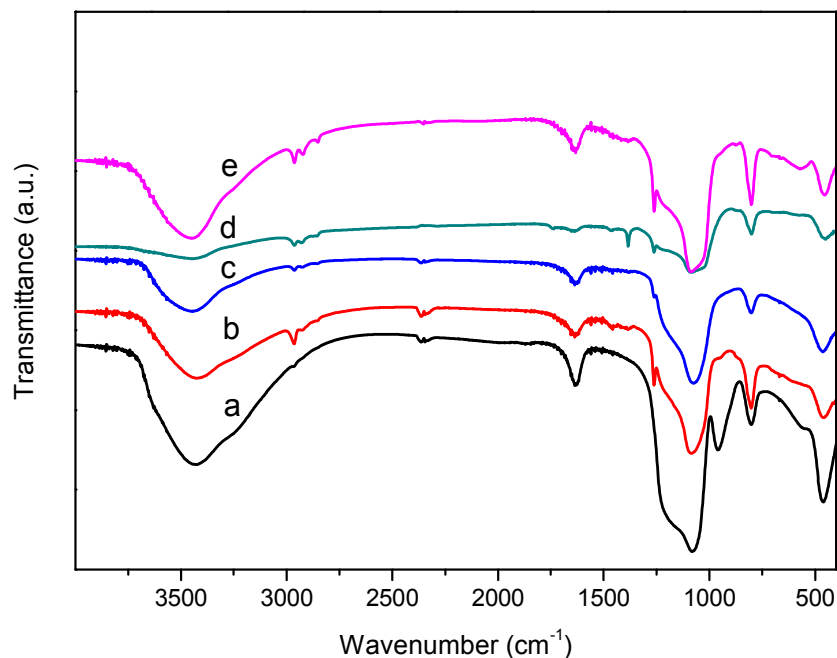


434
435

436 Fig. 8. FT-IR spectra of a) SBA-15 b) PADOH-HMDS-SBA-15 c) Ti-PADO-HMDS-
437 SBA-15 d) Zn-PADO-HMDS-silica e) Zn-PADO-HMDS-SBA-15 f) Mg-PADO-
438 HMDS-SBA-15 and g) Al-PADO-HMDS-SBA-15.

439 Fig. 9 shows the spectra of those materials prepared by direct immobilization of
440 $\text{Ti}(\text{O}^i\text{Pr})_4$, ZnMe_2 , $\text{Al}(\text{O}^i\text{Pr})_3$ or $\text{Mg}(\text{O}^n\text{Bu})_2$ on the previously dehydrated silica surface.
441 All spectra have in common the presence of $\nu(\text{C-H})$ stretching vibrations in the range
442 $2858\text{--}2962\text{ cm}^{-1}$ which supports the presence of ligands, alkoxy or alkyl chains, directly
443 bonded to the metal atoms. For Ti-SBA-15 and Al-SBA-15 the bands typical of
444 isopropoxy groups bonded to metal anchored complexes appear at 1466 cm^{-1} ($\delta_a(\text{CH}_2)$,
445 $\delta_a(\text{CH}_3)$), and 1385 cm^{-1} $\delta_s(\text{CH}_3)$; meanwhile the presence of a band at 950 cm^{-1} is clear
446 evidence of the presence of Ti anchored onto the silica surface, since this absorption is
447 due to the antisymmetric Ti-O-Si stretching vibration. As previously reported, grafting
448 reactions of isopropoxy titanium and aluminium complexes may occur with different
449 possible stoichiometries; through tripodal, bipodal and monopodal connections, the
450 proportion of them depending on the metal content.³⁵ The spectra obtained for Zn and
451 Mg-SBA-15 suggest the presence of different type of species grafted onto the silica

452 surface, naked magnesium and zinc species, as well as, butyl magnesium and methyl
453 zinc grafted complexes.

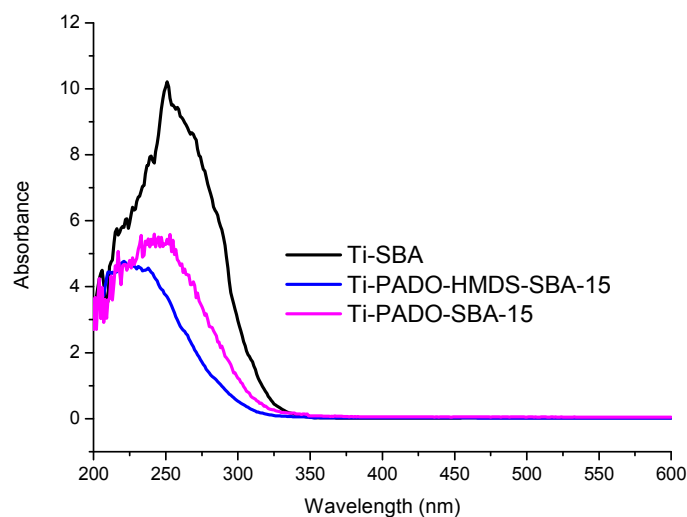


454 Fig. 9. FT-IR spectra of a) SBA-15 b) Ti-SBA-15 c) Zn-SBA-15 d) Mg-SBA-15 e) Al-
455 SBA-15.
456

457

458 Diffuse reflectance UV-vis spectroscopy (DRUV-vis) is a useful corroborative tool
459 in indicating the coordination environment of titanium sites. Absorption maxima in the
460 range of 210-240 nm are attributed to a LMCT for true four-coordinate Ti (IV). The
461 titanium grafted samples Ti-SBA-15 spectrum (taken under ambient air conditions, Fig.
462 10) shows a broad absorption band in the range 210-300 nm, with a maximum at 250
463 nm. It has been observed that the ligand-metal charge transfer transition red shifted with
464 increasing TiO₂ suggests a gradual increase in the polymerization degree of titanium
465 atoms. Based on these findings it can be deduced that the titanium atoms are mainly
466 grafted on the wall surface of the SBA-15 by one or two O-Si-O bridges as
467 Ti(OSi)(OR)₃ or Ti(OSi)₂(OR)₂ in partially polymerized states.³⁶ The DRUV-vis
468 spectrum of Ti-PADO-HMDS-SBA-15 exhibits a broad band in the range 240-210 nm,
469 at $\lambda_{\text{max}} = 210$ nm for the oxygen to tetrahedral Ti(IV) charge transfer band (LMCT) and
470 higher wavenumber values indicative of the presence of a second type of titanium

471 species with higher coordination environments as expected due to the existence of an
472 additional nitrogen donor atom in the ligand skeleton. For Ti-PADO-SBA-15 a shift of
473 the broad band to higher wavenumber value is observed (see Fig. 10). This behaviour
474 has been observed previously by our group,³⁷ it seems to be that the steric crowding
475 imposed by the trimethylsilyl groups attached to the silica surface yields spatially
476 separated aminediol propyl units that behave as if they are isolated on the surface.
477 However, in absence of the protector the aminediol units attached to flexible alkyl
478 chains may be near enough to allow some degree of oligomerization between metallic
479 units given the higher amount of titanium in this material and the tendency of this metal
480 to saturate its binding sphere. Therefore, it is probable that in some of the titanium
481 complexes on the silica surface the central core consists of an inter-linked titanium
482 isopropoxy moiety as observed frequently for these types of derivatives.³⁸ These results
483 confirm that when direct reaction between silanol groups on the surface and the metal
484 centre occurs multiple types of sites are often formed, removing the single site nature of
485 the system. The process that immobilizes the complex via a covalent linkage between
486 the ligand and the support using a multistep grafting approach seems to be a good
487 method to obtain well defined active centres (see Fig. 7c).



488

489 Fig. 10. DRUV-Vis spectra of Ti-SBA-15, Ti-PADO-SBA-15 and Ti-PADO-HMDS-
490 SBA-15.

491 **ϵ -Caprolactone polymerization with homogeneous and supported catalysts**

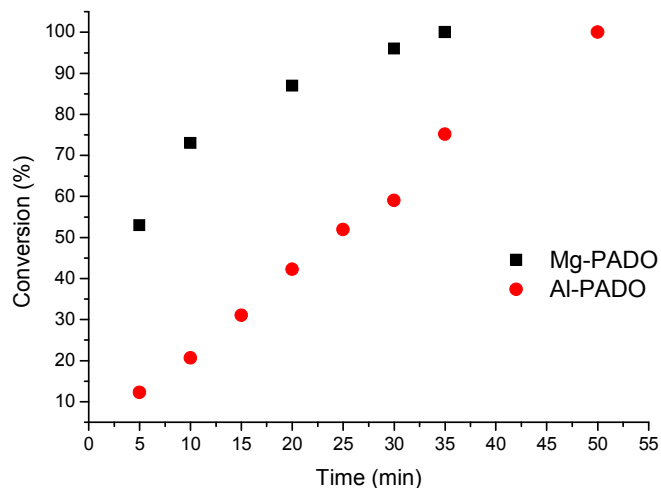
492

493 The ROP of ϵ -CL was carried out with homogeneous catalysts prepared by reaction
494 of an EtOH solution of 3-[Bis(2-hydroxyethyl)amino]propyl-triethoxysilane] with
495 Al(OⁱPr)₃, AlMe₃, Mg(ⁿBu)₂, Ti(OⁱPr)₄ or ZnMe₂, in dry toluene in 1:1 ratio. The
496 obtained species labelled as M-PADO (M=Al, Mg, Ti and Zn) have been characterized
497 via NMR and FT-IR spectroscopy (See supplementary information and Fig. S5-10).

498

499 The catalytic behaviour of M-PADO systems towards ROP of ϵ -CL in toluene
500 solution has been systematically examined; the results are reported in Table 4. The
501 polymerization proceeds at room temperature in the absence of an alcohol acting as co-
502 initiator. The process is straightforward for titanium with a 60% conversion after 24 h
503 and more efficient for zinc and aluminium complexes in monomer/initiator ratio 100:1,
504 achieving complete conversion at room temperature in 30 min (Fig. S11). Mg-PADO
505 exhibits the highest activity, 100% conversion in 5 min. Nevertheless, Al-PADO
506 provides the highest molecular weight and lowest PDI value ($M_n = 22200$, PDI = 1.22).
507 However, relatively high PDIs (1.22–1.45) of the polymers implied that side reactions
508 such as transesterification reactions exist in the polymerization process. Fig. 11 shows
509 the conversion *vs* time curves of ϵ -caprolactone polymerization ($M_0/I_0 = 300$) with Al
510 and Mg-PADO complexes. Both polymerizations proceed up to 100% conversion in a
511 different range of time. Metal complexes required a longer time to catalyze complete
512 polymerization when the monomer-to catalyst ratio increases. GPC analysis reveal that
513 the poly(ϵ -caprolactone) obtained shows values ranging from 9500 to 22200. Figure 11
514 also reveals some differences between the behaviour of both catalysts; unexpectedly the
515 conversion values for Al-PADO show a linear dependence with time, suggesting that
516 reaction is zero-order in monomer. In addition, the kinetic studies show a linear
517 relationship of $\ln(100-C(\%))$ *versus* time for Mg-PADO indicating that the
518 polymerization is first-order in monomer, which is consistent with the living character
519 of this polymerization. The curvature in the kinetic plot obtained for Al-PADO system
520 suggests a slow initiation of the process. This behaviour has previously been observed
521 for aluminium and lanthanide alkoxy derivatives;^{39,40} the existence of the aggregation
522 process of the active species in the polymerization medium slows the initiation step,
523 however, for higher degrees of monomer conversion the less reactive species eventually

524 transformed almost completely into the growing species. The apparent rate constants
525 were calculated as 10^{-4} min^{-1} for Zn-PADO complex at $(M_0/I_0) = 200$ (Fig. S12), and
526 0.118 min^{-1} for Mg-PADO complexes at $(M_0/I_0) = 300$ (Fig. S13)''



527

528 Fig. 11. Conversion *versus* reaction time for the polymerization of ϵ -CL ($[M_0/I_0] = 300$,
529 room temperature) initiated with Mg and Al-PADO complexes.

530

531

532

533 Table 4. Polymerization of ϵ -CL catalysed by M-PADO complexes^a

Initiator	Monomer/initiator	Conversion (%) ^b	Time (min)	M _n	PDI ^c
Al-PADO	100:1	100	30	11100	1.27
Al-PADO	200:1	100	50	20600	1.29
Al-PADO	300:1	100	60	22200	1.22
Mg-PADO	100:1	100	5	9200	1.32
Mg-PADO	200:1	100	30	10700	1.33
Mg-PADO	300:1	100	35	11100	1.33
Ti-PADO	100:1	60	1440	15200	1.42
Zn-PADO	100:1	100	30	9500	1.32
Zn-PADO	200:1	100	1440	---	---

534 ^aReaction conditions: 100 mg of homogenous catalyst, room temperature, toluene as solvent ^bDetermined by ¹H NMR analysis. ^cMeasured by
535 GPC at 27 °C in THF relative to polystyrene standards.

536

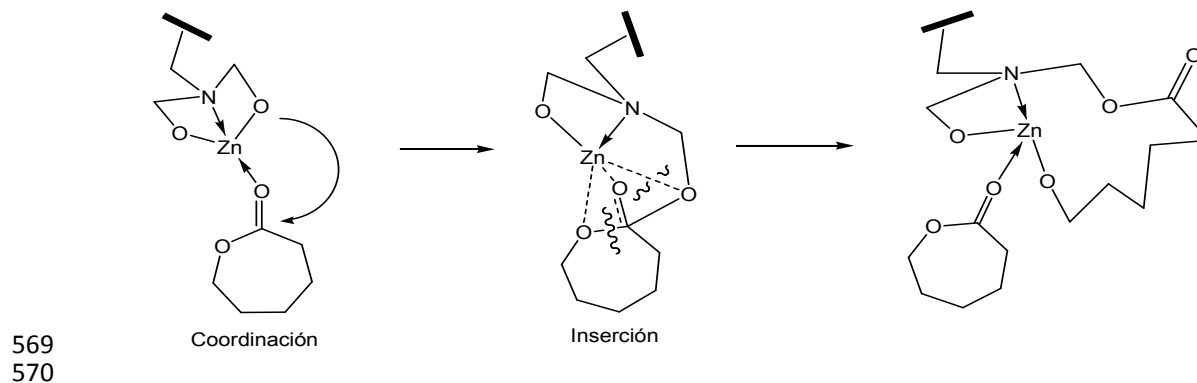
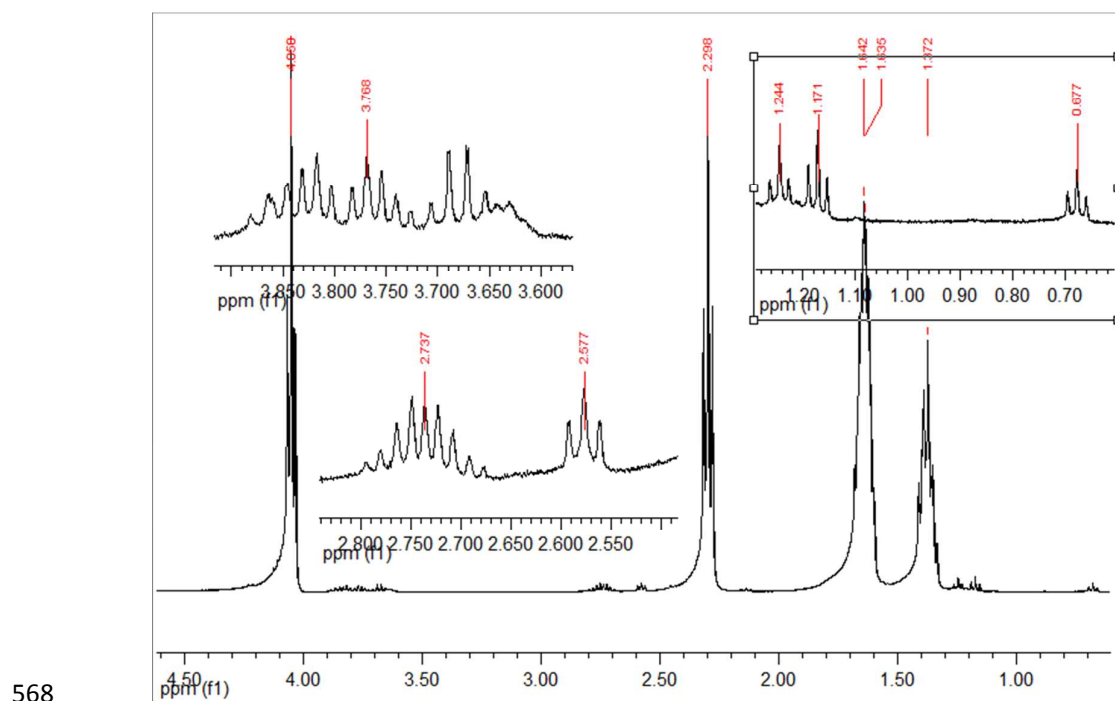
537 Table 5. Polymerization of ϵ -CL in presence of supported catalysts^a

Initiator/Co-initiator	Conversion (%) ^b	M_n	PDI ^c
Al-SBA-15	100	37900	1.44
Mg-SBA-15/BnOH	12	---	---
Ti-SBA-15	100	6900	1.20
Zn-SBA-15	47	5000	1.09
Al-PADO-HMDS-SBA-15	11	---	---
Mg-PADO-HMDS-SBA-15/BnOH	100	<3000	---
Ti-PADO-HMDS-SBA-15	10	---	---
Zn-PADO-HMDS-SBA-15	60	5100	1.11
Zn-PADO-HMDS-Silica	35	4200	1.19

538 ^aReaction conditions: 100 mg of heterogeneous catalyst, $[M_0/I_0] = 100$, temperature =80 °C, toluene as solvent, reaction time 24 h. ^aDetermined
539 by ¹H NMR spectroscopy analysis. ^bMeasured by GPC at 27 °C in THF relative to polystyrene standards

540 Previous studies with titanium and aluminium alkoxy complexes showed that the
541 ring opening polymerization of ϵ -caprolactone proceeds via a coordination-insertion
542 reaction through the formation of a coordination complex between the lactone and the
543 initiator with interaction between the carbonyl group and the metal atom. Then, the ring
544 opening reaction occurs with a selective cleavage of the acyl-oxygen bond. To
545 corroborate such a mechanism in the titanium and aluminium case, the identification of
546 end groups of the synthesized polymer isolated at low conversion rate to enhance end
547 groups concentration, was carried out. We confirmed by ^1H NMR spectroscopy the
548 presence of signals corresponding to the $-\text{CH}_2\text{-OH}$ end group at 3.63 ppm in both
549 spectra. In the titanium case a signal attributed to the methyl groups of isopropyl ester
550 function ($-\text{COOCH}(\text{CH}_3)_2$) at 4.90 ppm is present indicating that the growing end
551 groups are isopropoxy groups bonded to titanium (Fig. S14). In the aluminium case,
552 EtOH present in the reaction media during the synthesis of the complex acts as initiator
553 forming and ethoxy group directly bonded to the metal centre; the mechanism end-
554 group analysis supports this proposal since in the ^1H NMR spectrum of isolated ϵ -PCL a
555 triplet due to the methyl and methylene group of the ethyl ester function as growing end
556 group appears at 1.21 and 4.08 ppm, respectively (Fig. S15). The ROP polymerization
557 process using the magnesium complex as catalysts seems to proceed in a similar way,
558 the presence of EtOH during the synthesis procedure guarantees its coordination to the
559 magnesium centre, the growing end group is an ethyl ester function which is confirmed
560 by the ^1H NMR spectrum of the isolated polymer (Fig. S16).

561 Fig. 12 shows the ^1H NMR spectrum of a PCL polymer obtained by using Zn-
562 PADO as initiator by taking an aliquot of the toluene solution without previous
563 hydrolysis. As well as signals due to the protons along the polymer backbone, signals
564 due to the polymer's end groups can also be observed. The signals at 1.17–1.24, 2.57
565 and 2.73 ppm indicate that the PCL is probably attached with a $-\text{OCH}_2\text{N-CH}_2\text{-CH}_2\text{-}$
566 group, which suggests, in principle, the behaviour of the ancillary ligand as alkoxy
567 growing group and ROP may not be regarded as a living one.

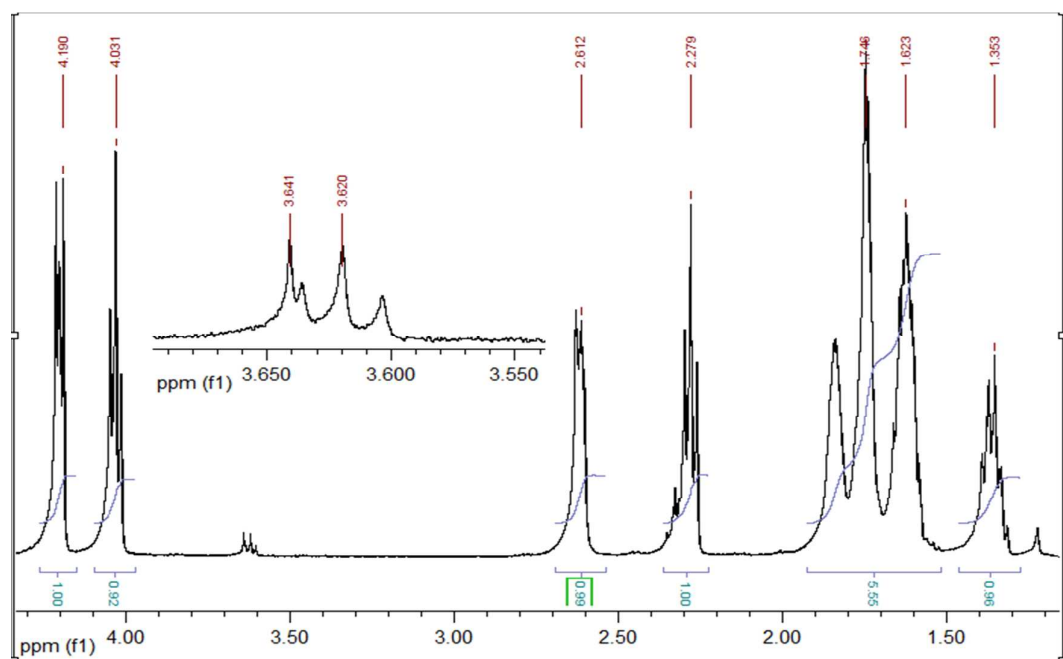


571 Fig. 12. ^1H NMR spectrum (measured in CDCl_3 , 400 MHz) of the polymer isolated
 572 from the polymerization of $\epsilon\text{-CL}$ initiated with Zn-PADO ($M_0/I_0 = 100$, at r.t.). Proposed
 573 coordination insertion mechanism.

574 The results of $\epsilon\text{-CL}$ polymerization with heterogeneous catalysts are summarized in
 575 Table 5. As can be seen the active heterogeneous Ti-SBA-15, Zn-SBA-15 and Zn-
 576 PADO-HMDS-SBA-15 catalysts formed poly(ϵ -caprolactone) with lower PDI values
 577 than those achieved with the homogeneous catalysts. In addition, for M-SBA-15 (M=
 578 Ti, Zn, Al, Mg) supported catalyst, those materials prepared by direct reaction of an
 579 alkoxy complex, $\text{M}(\text{OR})_n$, (M = Ti, Al) show better conversion values with respect to
 580 those prepared using alkyl complexes, MR_n (M = Zn, Mg) as metallic precursors. In

581 fact, using Ti-SBA-15 or Al-SBA-15 as initiator 100% conversion is reached in 24
582 hours and the molecular weight of PLA produced with Al-SBA-15 is approximately 5.5
583 times higher than the PCL made with Ti-SBA-15 or Zn-SBA-15. Mg-SBA-15 material
584 is inactive for the polymerization under the experimental conditions studied, benzylic
585 alcohol is needed as co-initiator, but even in the presence of benzylic alcohol the
586 conversion values are very low (only 12%). This is probably due to initiation being
587 faster due to the presence of metal-OⁱPr bond in Ti and Al-SBA-15 as demonstrated by
588 using ¹H NMR to study the synthesized polymer (Fig. S17 and S18). After appropriate
589 work up with isopropanol and isolation the recovered polymers show a very narrow
590 molecular weight distribution and a symmetrical monomodal elution peak is observed,
591 which indicates the complete absence of residual silica in the recovered polymer (see
592 Fig S19).²²

593 The initiation mechanism can be unambiguously established as a coordination-
594 insertion mechanism via an acyl-oxygen bond cleavage due to identification of
595 isopropoxy –O-CH(CH₃)₃ and hydroxyl –CH₂-OH end groups of synthesized polymer.
596 In the system Zn-SBA-15 initiation could be assumed to occur via a Zn-OSi bond.⁴¹
597 Alternatively, the study by ¹H NMR spectroscopy of the so obtained polymer shows a
598 triplet at 3.62 ppm assigned to the hydroxyl end group, –CH₂-OH, and a singlet signal at
599 3.64 ppm which can be assigned to a methoxy group –OCH₃ on the other end (Fig. 13).
600 Since the presence of methyl groups bonded to grafted zinc atoms is supported by the
601 infrared studies, a nucleophilic attack onto the monomer by the methyl group cannot be
602 discarded.⁴²



603

604 Fig. 13. ^1H NMR spectrum (measured in CDCl_3 , 400 MHz) of the polymer isolated
 605 from the polymerization of $\epsilon\text{-CL}$ initiated with Zn-SBA-15 ($M_0/I_0 = 100$, at r.t.).

606 A kinetic study was carried out using Ti-SBA-15 material (Fig. S20). The
 607 conversion value increases gradually with time, which suggests the accessibility of the
 608 titanium centres and the absence of mass transfer limitations. In addition, the kinetic
 609 studies shows a linear relationship of $\ln(100-C(\%))$ versus time (Fig. S21). The linearity
 610 obtained indicated that the polymerization is first-order in monomer, which is consistent
 611 with the living character of this polymerization.

612 In comparison the tethered systems show better conversion values in the case of Zn-
 613 PADO-HMDS-SBA-15 (with a conversion of 60% after 24 h) and Mg-PADO-HMDS-
 614 SBA-15 (with a conversion of 100% after 24 h), the latter in the presence of a benzylic
 615 alcohol as co-initiator. On the contrary, Ti and Al-PADO-HMDS-SBA-15 are shown to
 616 be very poor catalysts. Molecular weights of polymer produced by the most active zinc
 617 and aluminium heterogeneous systems decrease in comparison with their homogeneous
 618 counterparts. A remarkable fact is that Zn-PADO-HMDS-SBA-15 catalyst exhibited
 619 higher polymerization activity ($\text{TOF} = 2.5 \text{ h}^{-1}$) than Zn-PADO-HMDS-Silica catalyst
 620 ($\text{TOF} = 1.5 \text{ h}^{-1}$). In addition, the PCL obtained by using Zn-PADO-HMDS-SBA-15
 621 catalyst presents higher molecular weight and slightly lower polydispersity index
 622 compared with that achieved with Zn-PADO-HMDS-Silica. These results suggest that
 623 the properties of support may play an important role in the polymerization reaction.

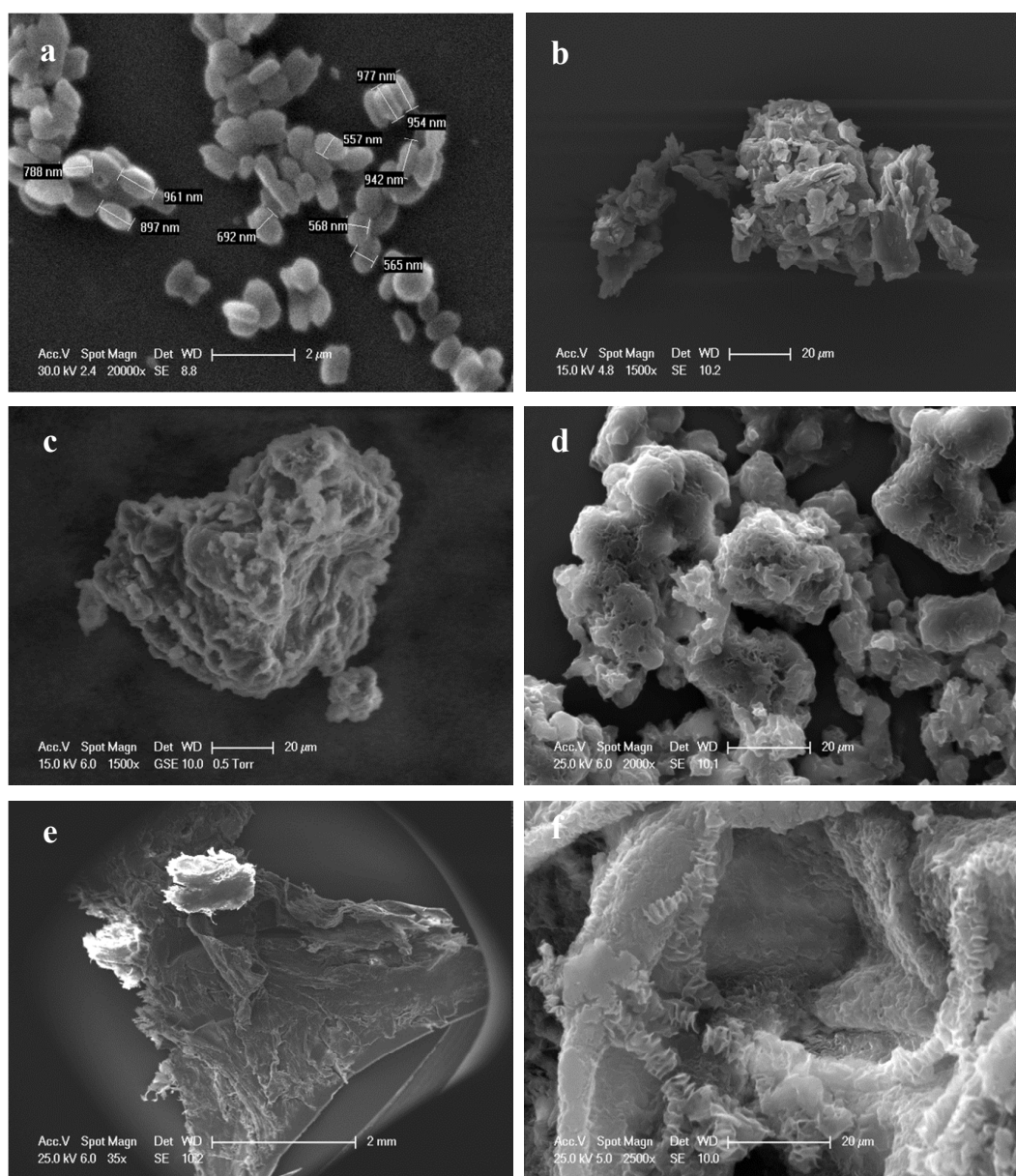
624 The end group analysis of the polymer obtained using Zn-PADO-HMDS-SBA-15
625 as initiator was conducted (Fig. S22). Since the only significant signal observed in the
626 ^1H NMR spectrum is the triplet assigned to the hydroxyl end group, a similar
627 mechanism to those observed for the homogeneous system is proposed the nucleophilic
628 attack on the monomer by the ancillary chelated ligand. Finally, the mechanism for
629 polymerization process using Mg-PADO-HMDS-SBA-15 as catalyst and benzylic
630 alcohol as co-initiator has been studied in a similar way (Fig. S23). In this case in the ^1H
631 NMR spectra a singlet signal appears at 5.05 ppm attributed to the methylene group of
632 the $-\text{O}-\text{CH}_2-\text{Ph}$ capped benzyl alcoxyl group, demonstrating the existence of a
633 coordination-insertion mechanism as well.

634 The polymers produced with the most active catalysts have been study by scanning
635 electron microscopy. The morphologies of PCL produced by Ti-SBA-15 (Fig. 14b) and
636 Zn-PADO-HMDS-SBA-15 (Fig. 14c) are irregular demonstrating that there is no
637 replication phenomenon, common in the heterogeneous polymerization of olefins. As
638 can be seen in Fig. 14a the particle is clearly an assembly of smaller structures, which
639 supports the presence of the active sites on the silica surface; monomer diffuses through
640 the pores of SBA-15 adsorbs on the layer of the polymer surrounding the catalyst and
641 diffuses through this layer to the active sites on the surface where polymerization takes
642 place.⁴³ On comparison, polymer morphology obtained by the homogeneous complex
643 Zn-PADO (Fig. 14d) is also irregular, supporting the existence of comparable active
644 single sites on the silica surface when using Zn-PADO-HMDS-SBA-15 (Fig. 14c).

645 The morphology of the more flexible polymer obtained by using Al-SBA-15 (Fig.
646 14e and 14f) as catalyst is very different as expected taking into account the higher
647 molecular weight of this material. Irregular folded layers are observed.

648

649



650

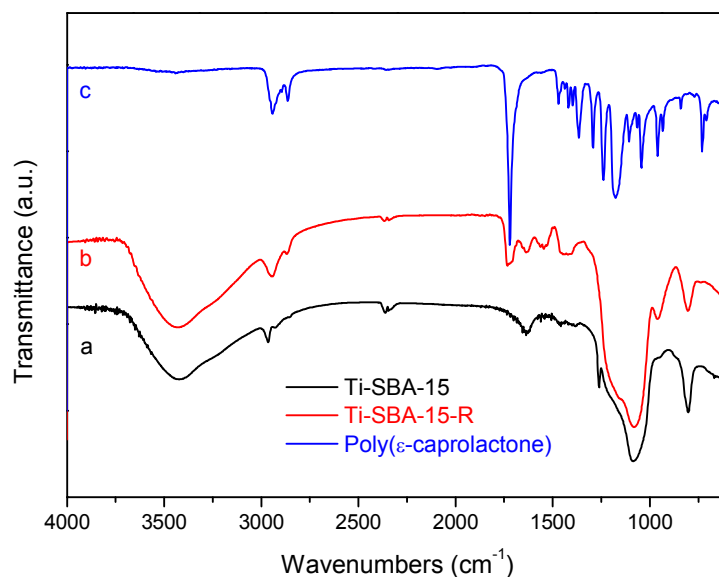
651 Fig. 14. SEM micrographs of a) SBA-15 b) PLC produced by Ti-SBA-15 c) PLC
 652 produced by Zn-PADO-HMDS-SBA-15 d) PLC produced by Zn-PADO e) and f) PLC
 653 produced by Al-SBA-15

654

655 A recycling experiment has been performed with Ti-SBA-15 by adding isopropanol
 656 to the polymerization medium when the monomer conversion is complete. The addition
 657 of alcohol has two roles: release of the polymer and regeneration of the isopropoxy
 658 groups bonded to titanium on the silica surface. In a first step PCL was initiated by

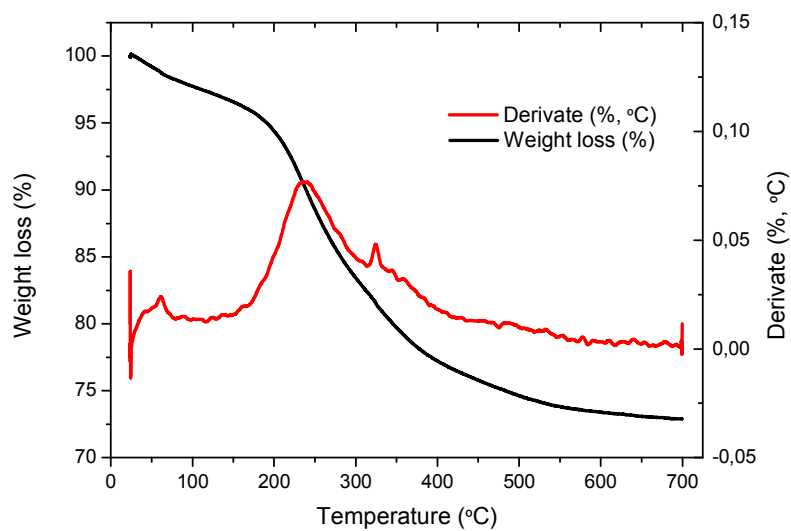
35

659 using Ti-SBA-15 in toluene at 80 °C, after 24 h monomer conversion, isopropanol was
660 added to the living polyester chains in order to separate them from the support and the
661 solid catalyst was allowed to settle. The supernatant polymer solution was separated by
662 filtration and the catalyst was washed with dichloromethane and dried under vacuum.
663 The ϵ -CL polymerization was repeated under similar experimental conditions by using
664 the recovered Ti-SBA-15 and it was possible to achieve 72% conversion, which
665 confirms the reusability of the catalyst. The stability of reused Ti-SBA-15-R catalyst
666 was examined by FT-IR analysis. The FT-IR spectrum of Ti-SBA-15-R catalyst shows
667 bands characteristic of SBA-15 and those corresponding to isopropoxy groups bonded
668 to titanium. In addition the band observed at 1724 cm^{-1} is attributed to the presence of
669 some amount of polymer (Fig. 15). Thermogravimetric analysis of recovered Ti-SBA-
670 15-R catalyst (Fig. 16) shows a weight loss in the range 185-350 °C attributed to the
671 degradation of isopropoxy ligands bonded to the titanium centre supporting the catalysts
672 regeneration. The TG curve does not show thermal degradation between 376 °C and 480
673 °C which would correspond to PCL decomposition.⁴⁴ In addition, these experiments
674 suggest, firstly, that the decrease in the activity may be due to the small amount of
675 polymer bonded to titanium and secondly that the removal of metal residues in the
676 polymer chain is possible by adding alcohol after polymerization. Therefore, a pure
677 metal-free polymer product can be obtained.



678

679 Fig. 15. FT-IR spectra of a) Ti-SBA-15, b) Ti-SBA-15-R and c) Poly(ϵ -caprolactone).



680

681 Fig. 16. Thermogravimetric analysis of Ti-SBA-15-R

682

683 **Conclusions**

684 In toluene solution heterogeneous and homogeneous systems have demonstrated to
685 be active initiators for the ROP of ϵ -CL. The heterogeneous catalysts required
686 significantly longer reaction times than their homogeneous counterparts; this is
687 presumably due to mass transport effects in the solid-supported materials. The
688 heterogeneous Ti-SBA-15, Zn-SBA-15 and Zn-PADO-HMDS-SBA-15 catalysts
689 produced poly(ϵ -caprolactone) with a narrow molecular weight distribution, close to
690 one. The support plays an important role, as can be concluded by comparing Zn-PADO-
691 HMDS-SBA-15 and Zn-PADO-HMDS-Silica systems, the former showing higher
692 activity values and producing polymers with higher molecular weight and narrower
693 polydispersity. In addition, the recovery experiments carried out for Ti-SBA-15 system
694 show the reusability of heterogeneous catalysts.

695

696 **Acknowledgments**

697 We gratefully acknowledge financial support from the Ministerio de Educación y
698 Ciencia, Spain (Project CTQ2012-30762).

699

700 **References**

-
- 1 Green Paper Packaging and Sustainability: An open dialogue between stakeholders. European 2011.
<http://www.europen.be/index.php?action=onderdeel&onderdeel=5&titel=News+Room&categorie=1&item=121>
 - 2 S. Martinez-Diaz, N. Garcia-Giralt, M. Lebourg, J.-A. Gómez-Tejedor, G. Vila, E. Caceres, P. Benito, M. Monleón Pradas, X. Nogues, J. L. Gómez Ribelles, J. Carles Monllau, *Am. J. Sports Med.*, 2010, **38**, 3 509.
 - 3 H. Seyednejad, A. H. Ghassemi, C. F. van Nostrum, T. Vermonden, W. E. Hennink, *J. Control. Rel.*, 2011, **152**, 168.
 - 4 Y. Oda, H. Asari, T. Urakami, K. Tonomura, *J. Ferment. Bioeng.* 1995, **80**, 265.
 - 5 L. S. Naira, C. T. Laurencin, *Prog. Polym. Sci.* 2007, **32**, 762.
 - 6 I. Vroman, L. Tighzert. *Materials*, 2009, **2**, 307.
 - 7 K. M. Stridsberg, M. Ryner, A.-C. Albertsson, *Adv. Polym. Sci.* 2002, **157**, 42.
 - 8 J. Cayuela, V. B.-L., P. Cassagnau, A. Michel, *Macromolecules*, 2006, **39**, 1338.
 - 9 D. J. Darensbourg, P. Ganguly, D. Billodeaux, *Macromolecules*, 2005, **38**, 5406.
 - 10 T. M. Ovitt, G. W. Coates, *J. Am. Chem. Soc.*, 2002, **124**, 1316.
 - 11 D. J. Darensbourg, O. Karroonnirun, *Organometallics*, 2010, **29**, 5627.
 - 12 L. R. Rieth, D. R. Moore, E. B. Lobkovsky, G. W. Coates, *J. Am. Chem. Soc.*, 2002, **124**, 15239.
 - 13 L. Wang, H. Ma, *Macromolecules*, 2010, **43**, 6535.
 - 14 B. J. O'Keefe, L. E. Breyfogle, M. A. Hillmyer, W. B. Tolman, *J. Am. Chem. Soc.*, 2002, **124**, 4385.
 - 15 A. Otero, A. Lara-Sanchez, J. Fernandez-Baeza, C. Alonso-Moreno, I. Marquez-Segovia, L. F. Sanchez-Barba, J. A. Castro-Osma, A. M. Rodríguez, *Dalton Trans.*, 2011, **40**, 4687.
 - 16 C.-Y. Li, C.-J. Yu, B.-T. Ko, *Organometallics*, 2013, **32**, 172.
 - 17 A. K. Sutar, T. Maharana, S. Dutta, C. T. Chen, C. C. Lin, *Chem. Soc. Rev.*, 2010, **39**, 1724.
 - 18 J. Wu, T.-L. Yu, C.-T. Chen, C.-C. Lin, *Coord. Chem. Rev.* 2006, **250**, 602.
 - 19 A. Arbaoui, C. Redshaw, *Polym. Chem.*, 2010, **1**, 801.

-
- 20 E. Kim, E. W. Shin, I.-K. Yoo, J. S. Chung, *J. Molec. Catal. A: Chem.*, 2009, **298**, 36.
- 21 J. H. Khan, F. Schue, G. A. George, *Polym. Int.*, 2010, **59**, 1506.
- 22 E. Martin, P. Dubois, R. Jérôme, *Macromolecules*, 2003, **36**, 7094.
- 23 K. Tortosa, T. Hamaide, C. Boisson, R. Spitz, *Macromol. Chem. Phys.*, 2001, **202**, 1156.
- 24 K. Yu, C. W. Jones, *J. Catal.* 2004, **222**, 558.
- 25 C. D. Iulio, M. D. Jones, M. F. Mahon, D. C. Apperley, *Inorg. Chem.*, 2010, **49**, 10232.
- 26 C. D. Iulio, M. D. Jones, M. F. Mahon, *J. Organomet. Chem.* 2012, **718**, 96.
- 27 W. Long, C. S. Gill, S. Choi, C. W. Jones, *Dalton Trans.*, 2010, **39**, 1470.
- 28 N. Wanna, T. Kraithong, T. Khamnaen, P. Phiriyawirut, S. Charoenchaidet, J. Tantirungrotechai, *Catal. Commun.* 2014, **45**, 118.
- 29 M. Choi, W. Heo, F. Kleitz, R. Ryoo, *Chem. Commun.* 2003, 1340.
- 30 I. Hierro, Y. Pérez, M. Fajardo, *J. Solid. State. Electrochem.* DOI: 10.1007/s10008-014-2496-x.
- 31 P. Zarabadi-Poor, A. Badiei, B. D. Fahlman, P. Arab, G. Mohammadi Ziarani, *Ind. Eng. Chem. Res.*, 2011, **50**, 10036.
- 32 R. Ballesteros, Y. Pérez, M. Fajardo, I. Sierra, I. Hierro, *Microporous Mesoporous Mater.*, 2008, **116**, 460.
- 33 P. Soubayrol, G. Dana, P. P. Man, *Magn. Reson. Chem.*, 1996, **34**, 638.
- 34 E. Pretsch, T. Clero, J. Seibl, W. Simon, *Tablas para la elucidación estructura de compuestos orgánicos por métodos espectroscópicos*, Ed. Alhambra1980.
- 35 P. Iengo, G. Aprile, M. D. Serio, D. Gazzoli, E. Santacesari, *Appl. Catal. A*, 1999, **178**, 97.
- 36 J. E. Haskouri, S. Cabrera, M. Gutierrez, A. Beltrán-Porter, D. Beltrán-Porter, M. D. Marcos, P. Amorós, *Chem. Commun.* 2001, 309.
- 37 P. G. Lampman, G. Kriz, *Introduction to spectroscopy*, Harcourt College Publishers, USA, 2001.
- 38 A. O. Bouth, G. L. Rice, S. L. Scott., *J. Am. Chem. Soc.* 1999, **121**, 7201.
- 39 B. M. Chamberlain, B. A. Jazdzewski, M. Pink, M. A. Hillmyer, W. B. Tolman. *Macromolecules*, 2000, **33**, 3970.
- 40 A. Kowalski, A. Duda, S. Penczek, *Macromolecules*, 1998, **31**, 2114.

-
- 41 M. D. Jones, M. G. Davidson, C. G. Keir, A. J. Wooles, M. F. Mahon, D. C. Apperley, *Dalton Trans.*, 2008, 3655.
- 42 M. Vivas, J. Contreras, *Eur. Polym. J.*, 2003, **39**, 43.
- 43 T. F. McKenna, J. B. P. Soares, *Chem. Eng. Sci.*, 2001, **56**, 3931.
- 44 A. Mohamed, V. L. Finkenstadt, S. H. Gordon, G. Biresaw, P. Debra E., P. Rayas-Duarte, *J. Appl. Polym. Sci.* 2008, **110**, 3256.